Inorg. Chem. **2009**, *48*, 1158−1167

One-Dimensional Co^{II} and Cu^{II} Coordination Polymers and a Discrete Cu^{II}_4 Complex of Carboxylate-Appended (2-Pyridyl)alkylamine Ligands: Spin-Canting and Anti-/Ferromagnetic Coupling

Himanshu Arora,[†] Francesc Lloret,[‡] and Rabindranath Mukherjee*[,†]

Department of Chemistry, Indian Institute of Technology Kanpur, Kanpur 208 016, India, and Departament de Química Inorgànica/Instituto de Ciencia Molecular (ICMOL), Universidad de València, Polígono de la Coma, s/n, 46980-Paterna (València), Spain

Received May 13, 2008

Structural characterization of the newly synthesized complexes $[M^{II}(L^1OO)(xH_2O)][ClO_4]\cdot 2H_2O$ [M = Co, $x = 1$ (**1**); M = Cu, $x = 0$ (**2**); $L^1OO^- = 3$-[(2-(pyridin-2-yl)ethyl){2-(pyridin-2-yl)methyl}amino]propionate] reveals that **1** and **2** are 1D chainlike coordination polymers. A tridentate variety of this ligand afforded a discrete tetranuclear complex $\{[Cu^{II}(L^2OO)(OClO_3)]\}_4\cdot MeCN$ (**3**) [$L^2OO^- = 3$-[*N*-methyl-{2-(pyridine-2-yl)ethyl}amino]propionate]. Analysis of the crystal packing diagrams reveals extensive $\pi-\pi$ stacking in **1** and C−H···O hydrogen bonding interactions in **3**, leading to the formation of network structures. For these complexes, absorption spectral properties have been investigated. All three complexes exhibit exchange interaction between the M^{II} ions through a syn−anti bridging carboxylate pathway. Magnetic studies on **1** show spontaneous magnetization below 5 K, which corresponds to the presence of spin-canted antiferromagnetism. At $T = 2$ K, the values of coercive field (H_c) and remnant magnetization (M_r) are 200 G and 0.019 μ_B, respectively. Analysis of the magnetic data through spin Hamiltonians in the form $\hat{H} = \sum_{i<j}^{n} -J_{ij}\hat{S}_i\hat{S}_j$ (J is positive for a ferromagnetic interaction and negative for an antiferromagnetic interaction) leads to the following set of best-fit parameters: $J = -2.65(2)$, $-0.66(1)$, and $+12.2(2)$ cm^{-1} for **1**, **2**, and **3**, respectively. An attempt has been made to rationalize the observed magnetic behavior.

Introduction

The design and synthesis of coordination polymers, based on transition-metal ions bridged by carboxylate groups, to fabricate low-dimensional molecule-based magnetic materials are currently under intense investigation.[1−3] Because of the dynamic nature of the metal−ligand bonds; various coordination geometries of the metal centers; nature and coordinating topologies of the ligands used; metal−ligand ratio; nature of the counterions; and various experimental conditions such as the solvents, temperature, and crystallization methods influence the final supramolecular assemblies formed. The increasing interest in this field is justified by the intellectual challenge in controlling and manipulating the self-assembly process.[4,5] In order to make a coordination polymer, it is, in principle, only necessary to react a potentially bridging ligand with a metal ion which has more than one vacant or labile site. Either infinite extended polymeric or discrete closed oligomeric structures can arise, depending on the nature of the system used.[6,7] The construction of coordination networks containing metal ions with magnetic anisotropy is particularly attractive because of the magnetic properties.[8,9] In order for such coordination polymers to be potentially useful, it is essential that their structures be capable of rational and predictable tuning via variation and functionalization of their constituent building blocks.

* To whom correspondence should be addressed. Tel.: +91-512-2597437. Fax: +91-512-2597436. E-mail: rnm@iitk.ac.in.
† Indian Institute of Technology Kanpur.
‡ Universidad de València.

(1) Kahn, O. *Molecular Magnetism*; VCH Publishers: New York, 1993.
(2) (a) Kahn, O. *Acc. Chem. Res.* **2000**, *33*, 647–657. (b) Miller, J. S.; Manson, J. L. *Acc. Chem. Res.* **2001**, *34*, 563–570. (c) Verdaguer, M. *Polyhedron* **2001**, *20*, 1115–1128. (d) Gatteschi, D.; Sessoli, R. *Angew. Chem., Int. Ed.* **2003**, *42*, 268–297. (e) Oshio, H.; Nakano, M. *Chem.—Eur. J.* **2005**, *11*, 5178–5185. (f) Miller, J. S. *Dalton Trans.* **2006**, 2742–2749.
(3) Tasiopoulos, A. J.; Vinslava, A.; Wernsdorfer, W.; Abboud, K. A.; Christou, G. *Angew. Chem., Int. Ed.* **2004**, *43*, 2117–2121.
(4) (a) Murray, K. S. *Adv. Inorg. Chem.* **1995**, *43*, 261–358. (b) Winpenny, R. E. P. *Adv. Inorg. Chem.* **2001**, *52*, 1–111.
(5) (a) Janiak, C. *Dalton Trans.* **2003**, 2781–2804. (b) Kitagawa, S.; Kitaura, R.; Noro, S.-i. *Angew. Chem., Int. Ed.* **2004**, *43*, 2334–2375.

10.1021/ic800861m CCC: $40.75
Published on Web 01/07/2009

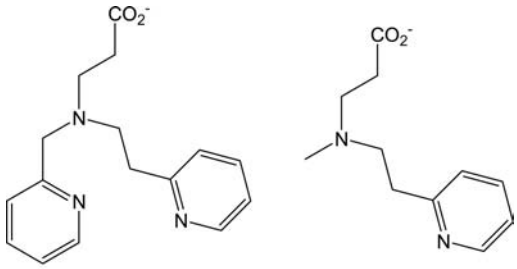

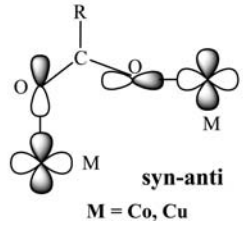

In continuation of our efforts on new magnetic systems[10] and from the above perspective, here we have used a new unsymmetrical (2-pyridyl)alkylamine-based tetradentate ligand with a flexible carboxylate linker, the lithium salt of 3-[(2-(pyridin-2-yl)ethyl){2-(pyridin-2-yl)methyl}amino]-propionic acid ($L^1OO^-Li^+$), to direct the geometry and dimensionality of the self-assembled network. Utilizing L^1OO^-, we have synthesized 1D coordination polymers of Co^{II} and Cu^{II}, with closely similar metal−ligand bonding characteristics. Within this framework of ligand topology, to pinpoint the effect of denticity of the ligands on the resultant complexes, we have used the Li salt of 3-[*N*-methyl-*N*-{2-(pyridin-2-yl)ethyl}amino]propionic acid ($L^2OO^-Li^+$) and synthesized a discrete tetracopper(II) complex. We present here the magneto-structural behavior of these complexes.

Experimental Section

Materials and Reagents. All reagents and solvents were obtained from commercial sources and used as received. Solvents were dried/purified following standard procedures. 2-(Pyridin-2-yl)-*N*-(pyridin-2-ylmethyl)ethanamine was prepared following a reported procedure.[11a] The methodology followed to prepare the ligands $L^1OO^-Li^+$ and $L^2OO^-Li^+$ was adapted from reported procedures.[11b,c]

Syntheses of Ligands. *N*-Methylpropanoate-*N*-2-pyridylmethyl-*N*-3-pyridyl-ethylamine (L^1OOMe). 2-(Pyridin-2-yl)-*N*-(pyridin-2-ylmethyl)ethanamine (3.50 g, 16.4 mmol) and methylacrylate (1.40 g, 16.6 mmol) were mixed in dry CH_3OH (30 mL) and refluxed for 14 h. After this period, removal of the solvent yielded the crude product as a brown oil, which was chromatographed on silica gel (60−120 mesh) with $CHCl_3$ as the eluent. The purified product was obtained as a brown oil. Yield: 3.00 g, ∼60%. ^{1}H NMR (80 MHz, $CDCl_3$): δ 8.63 (2H, d, pyridine H^6), 7.69 (2H, d, pyridine H^4), 7.32−6.97 (4H, m, pyridine $H^{3,5}$), 3.94 (2H, s, $-CH_2NC_5H_4$), 3.67 (3H, s, CO_2CH_3), 2.92 (4H, s, $-CH_2CH_2NC_5H_4$), 2.46 (2H, m, $-NCH_2CH_2CO_2CH_3$), 2.24 (2H, m, $-CH_2CO_2CH_3$).

Lithium Salt of 3-[(2-(Pyridin-2-yl)ethyl){2-(pyridin-2-yl)methyl}amino]propionic Acid ($L^1OO^-Li^+$). *N*-Methylpropanoate-*N*-2-pyridylmethyl-*N*-3-pyridylethylamine (3.50 g, 11.8 mmol) was dissolved in dry CH_3OH (25 mL), and to it was added solid LiOH (0.30 g, 12.5 mmol). The reaction mixture was stirred for two days at room temperature. The solvent was then removed under reduced pressure, and the product was obtained as a brown oil. Yield: 2.00 g, ∼58%. ^{1}H NMR (80 MHz, $CDCl_3$): δ 8.63 (2H, d, pyridine H^6), 7.69 (2H, d, pyridine H^4), 7.32−6.97 (4H, m, pyridine $H^{3,5}$), 3.94 (2H, s, $-CH_2NC_5H_4$), 2.92 (4H, s, $-CH_2CH_2NC_5H_4$), 2.46 (2H, m, $-NCH_2CH_2COO^-$), 2.24 (2H, m, $-CH_2COO^-$).

Methyl-3-(methyl(2-(pyridin-2-yl)ethyl)amino)propanoate (L^2OOMe). *N*-Methyl-2-(pyridin-2-yl)ethanamine (2.00 g, 14.7 mmol) and methyl acrylate (1.23 g, 14.7 mmol) were mixed in dry CH_3OH (20 mL) and refluxed for 20 h. The solvent was then removed under a vacuum to give a yellow oil. Yield: 2.00 g, ∼62%. ^{1}H NMR (in

(6) Selected examples of carboxylate-bridged coordination polymers: (a) Rettig, S. J.; Thompson, R. C.; Trotter, J.; Xia, S. *Inorg. Chem.* **1999**, *38*, 1360–1363. (b) Ruiz-Pérez, C.; Rodríguez-Martín, Y.; Hernández-Molina, M.; Delgado, F. S.; Pasán, J.; Sanchiz, J.; Lloret, F.; Julve, M. *Polyhedron* **2003**, *22*, 2111–2123. (c) Pasán, J.; Delgado, F. S.; Rodríguez-Martín, Y.; Hernández-Molina, M.; Ruiz-Pérez, C.; Sanchiz, J.; Lloret, F.; Julve, M. *Polyhedron* **2003**, *22*, 2143–2153. (d) Choi, K.-Y.; Jeon, Y.-M.; Ryu, H.; Oh, J.-J.; Lim, H.-H.; Kim, M.-W. *Polyhedron* **2004**, *23*, 903–911. (e) Noro, S.-I.; Miyasaka, H.; Kitagawa, S.; Wada, T.; Okubo, T.; Yamashita, M.; Mitani, T. *Inorg. Chem.* **2005**, *44*, 133–146. (f) Choi, K.-Y.; Park, S.-Y.; Jeon, Y.-M.; Ryu, H. *Struct. Chem.* **2005**, *16*, 649–656. (g) Pasán, J.; Sanchiz, J.; Ruiz-Pérez, C.; Lloret, F.; Julve, M. *Inorg. Chem.* **2005**, *44*, 7794–7801. (h) Zheng, Y.-Z.; Tong, M.-L.; Zhang, W.-X.; Chen, X.-M. *Angew. Chem., Int. Ed.* **2006**, *45*, 6310–6314. (i) Zhang, Y.; Liang, H.-C.; Zakharov, L. N.; Das, S. K.; Hetu, M. M.; Rheingold, A. L. *Inorg. Chim. Acta* **2007**, *360*, 1691–1701. (j) Rodríguez-Diéguez, A.; Cano, J.; Kivekäs, R.; Debdoubi, A.; Colacio, E. *Inorg. Chem.* **2007**, *46*, 2503–2510. (k) Liu, Y.-Y.; Ma, J.-F.; Yang, J.; Su, Z.-M. *Inorg. Chem.* **2007**, *46*, 3027–3037. (l) Żurowska, B.; Ślepokura, K. *Inorg. Chim. Acta* **2008**, *361*, 1213–1221. (m) Yang, B.-P.; Prosvirin, A. V.; Guo, Y.-Q.; Mao, J.-G. *Inorg. Chem.* **2008**, *47*, 1453–1459.
(7) Selected examples of carboxylato-bridged tetracopper(II) complexes: (a) Colacio, E.; Costes, J.-P.; Kivekäs, R.; Laurent, J.-P.; Ruiz, J. *Inorg. Chem.* **1990**, *29*, 4240–4246. (b) Colacio, E.; Dominguez-Vera, J.-M.; Costes, J.-P.; Kivekäs, R.; Laurent, J.-P.; Ruiz, J.; Sundberg, M. *Inorg. Chem.* **1992**, *31*, 774–778. (c) Wang, S.; Trepanier, S. J.; Zheng, J.-C.; Pang, Z.; Wagner, M. J. *Inorg. Chem.* **1992**, *31*, 2118–2127. (d) Colacio, E.; Ghazi, M.; Kivekäs, R.; Moreno, J. M. *Inorg. Chem.* **2000**, *39*, 2882–2890. (e) Murugesu, M.; Clérac, R.; Pilawa, B.; Mandel, A.; Anson, C. E.; Powell, A. K. *Inorg. Chim. Acta* **2002**, *337*, 328–336. (f) Dey, S. K.; Bag, B.; Abdul Malik, K. M.; Salah El Fallah, M.; Ribas, J.; Mitra, S. *Inorg. Chem.* **2003**, *42*, 4029–4035.
(8) Carlin, R. L. *Magnetochemistry*; Springer-Verlag: Berlin, Heidelberg, 1986.
(9) Selected spin-canting systems: (a) Meyer, A.; Gleizes, A.; Girerd, J.-J.; Verdaguer, M.; Kahn, O. *Inorg. Chem.* **1982**, *21*, 1729–1739. (b) Martinez-Lorente, M.-A.; Tuchagues, J. P.; Pétrouléas, V.; Savariault, J.-M.; Poinsot, R.; Drillon, M. *Inorg. Chem.* **1991**, *30*, 3587–3589. (c) Hernández-Molina, M.; Lloret, F.; Ruiz-Pérez, C.; Julve, M. *Inorg. Chem.* **1998**, *37*, 4131–4135. (d) Armentano, D.; De Munno, G.; Lloret, F.; Palii, A. V.; Julve, M. *Inorg. Chem.* **2002**, *41*, 2007–2013. (e) Liu, T.-F.; Fu, D.; Gao, S.; Zhang, Y.-Z.; Sun, H.-L.; Su, G.; Liu, Y.-J. *J. Am. Chem. Soc.* **2003**, *125*, 13976–13977. (f) Zheng, L.-M.; Gao, S.; Yin, P.; Xin, X.-Q. *Inorg. Chem.* **2004**, *43*, 2151–2156. (g) Kim, J.; Han, S.; Pokhodnya, K. I.; Migliori, J. M.; Miller, J. S. *Inorg. Chem.* **2005**, *44*, 6983–6988. (h) Sun, Z.-M.; Prosvirin, A. V.; Zhao, H.-H.; Mao, J.-G.; Dubar, K. R. *J. Appl. Phys.* **2005**, *97*, 10B305-1–10B305-3. (i) Ko, H. H.; Lim, J. H.; Kim, H. C.; Hong, C. S. *Inorg. Chem.* **2006**, *45*, 8847–8849. (j) Li, J.-R.; Yu, Q.; Tao, Y.; Bu, X.-H.; Ribas, J.; Batten, S. R. *Chem. Commun.* **2007**, 2290–2292. (k) Yoon, J. H.; Lim, J. H.; Choi, S. W.; Kim, H. C.; Hong, C. S. *Inorg. Chem.* **2007**, *46*, 1529–1531. (l) Rodríguez-Diéguez, A.; Kivekäs, R.; Sakiyama, H.; Debdoubi, A.; Colacio, E. *Dalton Trans.* **2007**, 2145–2149. (m) Barrios, L. A.; Ribas, J.; Aromi, G.; Ribas-Ariño, J.; Gamez, P.; Roubeau, O.; Teat, S. J. *Inorg. Chem.* **2007**, *46*, 7154–7162. (n) Yuan, M.; Zhao, F.; Zhang, W.; Wang, Z.-M.; Gao, S. *Inorg. Chem.* **2007**, *46*, 11235–11242. (o) Rodríguez-Diéguez, A.; Palacios, M. A.; Sironi, A.; Colacio, E. *Dalton Trans.* **2008**, 2887–2893.
(10) Sharma, A. K.; Lloret, F.; Mukherjee, R. *Inorg. Chem.* **2007**, *46*, 5128–5130.

$CDCl_3$): δ 8.80 (d, 1H, py-H^6), 7.90−7.20 (m, 3H, py-$H^{3,4,5}$), 3.63 (s, 3H, $CH_2CH_2CO_2CH_3$), 2.85−2.65 (m, 4H, py-CH_2CH_2), 2.60−2.35 (m, 4H, $CH_2CH_2CO_2CH_3$), 2.10 (s, 3H, NCH_3).

Lithium Salt of 3-[*N*-Methyl-{2-(pyridin-2-yl)ethyl}amino]-propanic Acid ($L^2OO^-Li^+$). Methyl-3-(methyl(2-(pyridin-2-yl)ethyl)amino)propanoate (3.25 g, 14.7 mmol) was dissolved in dry CH_3OH (20 mL), and to it was added solid LiOH (0.35 g, 14.7 mmol). After stirring for 2 days, the solvent was removed under a vacuum to give a pale yellow oil. Yield: 1.80 g, ∼60%.^{1}H NMR (in $CDCl_3$): δ 8.80 (d, 1H, py-H^6), 7.90−7.20 (m, 3H, py-$H^{3,4,5}$), 2.85−2.65 (m, 4H, py-CH_2CH_2), 2.60−2.35 (m, 4H, $CH_2CH_2COO^-$), 2.15 (s, 3H, NCH_3).

Synthesis of Metal Complexes. $[Co^{II}(L^1OO)(H_2O)][ClO_4]\cdot 2H_2O$ (1). $L^1OO^-Li^+$ (0.15 g, 0.50 mmol) was dissolved in H_2O (10 mL), and to it was added solid $[Co^{II}(H_2O)_6][ClO_4]_2$ (0.18 g, 0.50 mmol). The reaction mixture was then refluxed for 3 h and kept for slow evaporation. After 4 days, a crystalline compound started coming out, which was suitable for structural characterization. Yield: 0.15 g, ∼60%.

Characterization of 1. Anal. calcd for $C_{16}H_{24}ClCoN_3O_9$: C, 38.67; H, 4.83; N, 8.46. Found: C, 38.57; H, 4.89; N, 8.51. IR (KBr, cm^{-1}, selected peaks): 3371 (ν(OH)); 1604 and 1439 ($\nu(OAc^-)$); 1088 and 630 ($\nu(ClO_4^-)$). Absorption spectrum [λ_{max}, nm (ε, M^{-1} cm^{-1})]: (in H_2O) 260 (5 650), 490 (20), 1050 (10).

$[Cu^{II}(L^1OO)][ClO_4]\cdot 2H_2O$ (2). $L^1OO^-Li^+$ (0.20 g, 0.67 mmol) was dissolved in H_2O (10 mL), and to it was added solid $[Cu^{II}(H_2O)_6][ClO_4]_2$ (0.25 g, 0.67 mmol). The blue solid that immediately formed was filtered and washed with cold water. The solid was recrystallized in a hot H_2O/CH_3CN (v/v, 1:1) mixture. Slow evaporation of the solvent afforded dark blue crystals, suitable for structural studies. Yield: 0.20 g, ∼60%.

Characterization of 2. Anal. calcd for $C_{16}H_{22}ClCuN_3O_8$: C, 39.75; H, 4.55; N, 8.69. Found: C, 39.26; H, 4.23; N, 8.97. IR (KBr, cm^{-1}, selected peaks): 3426 (ν(OH)); 1609 and 1443 ($\nu(OAc^-)$); 1088 and 627 ($\nu(ClO_4^-)$). Absorption spectrum [λ_{max}, nm (ε, M^{-1} cm^{-1})]: (in H_2O) 255 sh (15 050), 630 (110), 965 (30).

$\{[Cu^{II}(L^2OO)(OClO_3)]\}_4\cdot MeCN$ (3). $L^2OO^-Li^+$ (0.10 g, 0.46 mmol) was dissolved in H_2O (10 mL), and to it was added solid $[Cu^{II}(H_2O)_6][ClO_4]_2$ (0.17 g, 0.46 mmol). The reaction mixture was refluxed for 2 h and then kept for slow evaporation. After 5 days, a blue crystalline compound that separated was collected. Recrystallization was achieved by the vapor diffusion of Et_2O into a CH_3CN solution of the compound. Yield: 0.10 g, ∼60%.

Characterization of 3. Anal. calcd for $C_{46}H_{63}Cl_4Cu_4N_9O_{24}$: C, 36.27; H, 4.13; N, 8.28. Found: C, 36.29; H, 4.14; N, 8.28. IR (KBr, cm^{-1}, selected peaks): 2315 ($\nu(CN^-)$); 1611 and 1448 ($\nu(OAc^-)$); 1109 and 623 ($\nu(ClO_4^-)$). Absorption spectrum [λ_{max}, nm (ε, M^{-1} cm^{-1})]: (in CH_3CN) 260 (68 400), 290 sh (26 600), 635 (880).

Physical Measurements. Elemental analyses were obtained using a Thermo Quest EA 1110 CHNS-O (Italy). Spectroscopic measurements were made using the following instruments: IR (KBr, 4000−600 cm^{-1}), Bruker Vector 22; electronic, Perkin-Elmer Lambda 2 and Agilent 8453 diode-array spectrophotometers. ^{1}H NMR spectra ($CDCl_3$ solution) were obtained on either a Bruker WP-80 (80 MHz) or a JEOL JNM LA (400 MHz) spectrophotometer. Chemical shifts are reported in parts per million referenced to TMS.

Magnetic Measurements. The measurements were carried out (València) using a Quantum Design SQUID Magnetometer at 0.01 T for T < 50 K in order to avoid saturation effects and 0.1 T for T > 50 K. Diamagnetic corrections were estimated from Pascal's constants.

Table 1. Data Collection and Structure Refinement Parameters for $[Co^{II}(L^1OO)(H_2O)][ClO_4]\cdot 2H_2O$ (**1**), $[Cu^{II}(L^1OO)][ClO_4]\cdot 2H_2O$ (**2**), and $\{[Cu(L^2OO)(OClO_3)]\}_4\cdot MeCN$ (**3**)

	1	**2**[c]	**3**
chem formula	$C_{16}H_{24}ClCoN_3O_9$	$C_{16}H_8ClCuN_3O_8$	$C_{46}H_{60}Cl_4Cu_4N_9O_{24}$
fw	496.76	469.24	1518.99
cryst size/mm × mm × mm	0.2 × 0.2 × 0.1	0.2 × 0.2 × 0.1	0.2 × 0.1 × 0.1
temp/K	100(2)	100(2)	293(2)
λ/Å	0.710 73	0.710 73	0.710 73
cryst syst	monoclinic	monoclinic	tetragonal
space group	$P2_1/n$ (no. 14)	$P2_1/c$ (no. 14)	$P4/n$ (no. 85)
a/Å	15.172(5)	10.2179(14)	19.038(5)
b/Å	9.210(5)	8.6838(12)	19.038(5)
c/Å	15.419(5)	23.262(3)	8.374(4)
β/deg	107.108(5)	102.055(3)	90
V/Å^3	2059.20(15)	2018.5(5)	3035.1(18)
Z	4	4	2
d_{calcd}/g cm^{-3}	1.602	1.544	1.662
μ/mm^{-1}	1.018	1.261	1.644
F(000)	1028	940	1550
no. of reflns collected	13187	13028	19587
no. of ind. reflns [R (int)]	5085 (R_{int} = 0.0501)	4979 (R_{int} = 0.0751)	3766 (R_{int} = 0.1263)
No. of reflns used [$I > 2\sigma(I)$][a,b]	3734	3228	1875
GOF on F^2	1.073	1.150	1.074
Final R indices [$I > 2\sigma(I)$]	0.0652, 0.1452	0.1088, 0.2397	0.0953, 0.1821
final R indices (all data)	0.0975	0.1659	0.1946
	(0.1839)	(0.2758)	(0.2219)

[a] $R_1 = \sum(||F_o| - |F_c||)/\sum|F_o|$. [b] $wR_2 = \{\sum[w(|F_o|^2 - |F_c|^2)^2]/\sum[w(|F_o|^2)^2]\}^{1/2}$. [c] Hydrogen atoms associated with severely disordered atoms could not be located.

Crystal Structure Determination. Diffracted intensities were collected on a Bruker SMART APEX CCD diffractometer at 100(2) K (**1** and **2**) and at 293(2) K (**3**) using graphite-monochromated Mo Kα (λ = 0.71073 Å) radiation. Intensity data were corrected for Lorentz polarization effects. Empirical absorption correction (SADABS) was applied. The structures were solved by SIR-97, expanded by Fourier-difference syntheses, and refined with SHELXL-97, incorporated in the WinGX 1.64 crystallographic collective package.[12] Hydrogen atoms were placed in idealized positions and treated using riding model approximation with displacement parameters derived from those of the atoms to which they were bonded. All non-hydrogen atoms were refined with anisotropic thermal parameters by full-matrix least-squares procedures on F^2. The convergence was measured by the factors R and R_w, where $R = \sum(||F_o| - |F_c||)/\sum|F_o|$ and $R_w = \{\sum[w(F_o^2 - F_c^2)^2]/\sum[w(F_o^2)^2]\}^{1/2}$. Pertinent crystallographic parameters are summarized in Table 1. For **1**, some degree of disorder was observed with the ClO_4^- counteranion and metal-coordinated tertiary amine nitrogen atom.[13] Three oxygen atoms, O(5), O(6), and O(7), were distributed over two positions, and they were refined with site occupation factors of 0.60/0.40, 0.50/0.50, and 0.55/0.45, respectively. The donor atom

(11) (a) Mahapatra, S.; Gupta, N.; Mukherjee, R. *J. Chem. Soc., Dalton Trans.* **1992**, 3041–3045. (b) Bhattacharya, S.; Snehalatha, K.; Kumar, V. P. *J. Org. Chem.* **2003**, *68*, 2741–2747. (c) Carvalho, N. M. F.; Horn, A., Jr.; Faria, R. B.; Bortoluzzi, A. J.; Drago, V.; Antunes, O. A. C. *Inorg. Chim. Acta* **2006**, *359*, 4250–4258.
(12) Farrugia, L. J. *WinGX*, version 1.64; Department of Chemistry, University of Glasgow: Glasgow, 2003.
(13) Cotton, F. A.; Dikarev, E. V.; Wong, W.-Y. *Inorg. Chem.* **1997**, *36*, 3268–3276.

N(2) was also distributed over two positions, and they were refined with a site occupation factor of 0.70/0.30. The quality of the structure determination of **2** is poor, which may be due to the poor quality of the crystal chosen for data collection, and the poor data set obtained. Unfortunately, we could not grow single crystals of **2** that were any better than the one used for the present study, as they were the best we could acquire. For **2**, some degree of disorder was observed with the metal-coordinated tertiary amine nitrogen atom[13] and methylene carbon atoms. The donor atom N(2) atom was distributed over two positions, and they were refined with a site occupation factor of 0.65/0.35. Two methylene carbon atoms, C(7) and C(14), were distributed over two positions, and they were refined with site occupation factors of 0.65/0.35 and 0.65/0.35, respectively. Hydrogen atoms associated with distributed atoms could not be located/fixed because of severe disorder present in complex **2** (Figure S1, Supporting Information). Therefore, only the overall structural characteristics derived from this structure determination are reliable. Intermolecular contacts of $\pi\cdots\pi$ stacking and C−H···O were examined with the DIAMOND package.[14] C−H distances were normalized along the same vectors to the neutron derived values of 1.083 Å.[15]

Results and Discussion

Syntheses and Characterization of the Ligands and the Complexes. The ligands $L^1OO^-Li^+$ and $L^2OO^-Li^+$ were synthesized by Michael condensation of methylacrylate with corresponding amines in CH_3OH, followed by hydrolysis of methyl esters. The ligands were characterized by their ^1H NMR spectra. Reactions of $L^1OO^-Li^+$ with $[M^{II}(H_2O)_6][ClO_4]_2$ (M = Co, Cu) in a 1:1 molar ratio in H_2O readily afforded microcrystals of composition $[Co^{II}(L^1OO)(H_2O)][ClO_4]\cdot 2H_2O$ (**1**) and $[Cu^{II}(L^1OO)][ClO_4]\cdot 2H_2O$ (**2**). A similar reaction between $L^2OO^-Li^+$ and $[Cu(H_2O)_6][ClO_4]_2$ yielded $\{[Cu^{II}(L^2OO)(OClO_3)]\}_4\cdot MeCN$ (**3**). The identities of **1**−**3** were elucidated from physicochemical measurements [elemental analysis, IR, and UV−vis spectra (see below)] and X-ray crystal structure analysis (see below). In IR spectra, each complex displays bands of $\nu(CH_3COO^-)$ stretching vibrations of the coordinated acetate ion: 1604 cm^{-1} and 1439 cm^{-1} for **1**; 1609 cm^{-1} and 1443 cm^{-1} for **2**; 1611 cm^{-1} and 1448 cm^{-1} for **3**. The IR spectra also showed bands due to ionic ClO_4^- for complexes **1** and **2**, and coordinated ClO_4^- for complex **3**.

Description of the Structures. In order to confirm the structure of the complexes and mode of coordination of the ligands, single-crystal X-ray structure determination of the complexes was carried out. Selected bond lengths and bond angles are listed in Table 2.

$[Co^{II}(L^1OO)(H_2O)][ClO_4]\cdot 2H_2O$ (1) and $[Cu^{II}(L^1OO)][ClO_4]\cdot 2H_2O$ (2). Complexes **1** and **2** exhibit a closely similar structure. Perspective views of the metal coordination environment and 1D polymeric structure in the crystals of $[Co^{II}(L^1OO)(H_2O)][ClO_4]\cdot 2H_2O$ (**1**) and $[Cu^{II}(L^1OO)][ClO_4]\cdot 2H_2O$ (**2**) are presented in Figures 1 and 2, respectively. The ligand $L^1OO(-)$ acts as a tetradentate ligand toward a M^{II} ion and acts as a monodentate bridging ligand toward a neighboring M^{II} center. Each M^{II} ion is coordinated by an ethylpyridyl nitrogen N(1), a tertiary amine nitrogen N(2), a methylpyridyl nitrogen N(3), and a carboxylate oxygen O(1) from the ligand $L^1OO(-)$ and with (**1**)/without (**2**) an oxygen, O(3), of H_2O. The M^{II} ions are bridged by a carboxylate group [oxygen atom O(2#) belongs to the carboxylate of an adjacent molecule] to form a one-dimensional (1D) polymeric chain with an intramolecular Co···Co distance of 5.515(2) Å and Cu···Cu distance of 4.579(6) Å. The angles between trans atoms at the metal center are in the range 166.07(15)−173.2(5)° for **1** and 165.7(3)−167.5(3)° for **2**. The cis angles span wide ranges 76.7(2)−101.2(2)° for **1** and 73.4(6)−102.3(6)° for **2**. Thus, in **1**, appreciable distortion of the $Co^{II}N_3$(pyridylethylmethylamine)O_2(monodentate and bridging carboxylate)O(water) coordination environment from ideal geometry is

Table 2. Selected Bond Lengths (Å) and Angles (deg) in $[Co^{II}(L^1OO)(H_2O)][ClO_4]\cdot 2H_2O$ (**1**), $[Cu^{II}(L^1OO)][ClO_4]\cdot 2H_2O$ (**2**), and $\{[Cu(L^2OO)(OClO_3)]\}_4\cdot MeCN$ (**3**)

$[Co^{II}(L^1OO)(H_2O)][ClO_4]\cdot 2H_2O$ (**1**)			
Co−O1	2.089(3)	N2b−Co−O2[a]	173.2(5)
Co−O2[a]	2.089(3)	N3−Co−O2[a]	95.85(14)
Co−O3	2.148(3)	O2[a]−Co−O3	87.83(13)
Co−N1	2.116(4)	N1−Co−O3	88.14(13)
Co−N2a	2.226(9)	O3−Co−N2a	101.2(2)
Co−N2b	2.180(2)	O3−Co−N2b	98.9(5)
Co−N3	2.108(4)	N3−Co−O3	86.17(13)
C16−O1	1.262(5)	N1−Co−N2a	91.96(19)
C16−O2	1.255(5)	N1−Co−N2b	84.1(4)
Co···Co[a]	5.515 (2)	N1−Co−N3	166.07(15)
O1−Co−N1	91.67(14)	N2a−Co−N3	76.7(2)
O1−Co−N2a	90.7(2)	N2b−Co-N3	84.2(4)
O1−Co−N2b	92.9(5)	Co−O1−C16	129.2(3)
O1−Co−N3	96.50(13)	Co[b]−O2−C16	135.9(3)
O1−Co−O2[a]	80.36(12)	O1−C16−O2	124.5(4)
O1−Co−O3	168.09(13)	O1−C16−C15	119.1(4)
N1−Co−O2[a]	96.63(15)	O2−C16−C15	116.4(4)
N2a−Co−O2[a]	167.7(2)		
$[Cu^{II}(L^1OO)][ClO_4]\cdot 2H_2O$ (**2**)			
Cu−O1	2.012(5)	O2−Cu−N1	98.0(2)
Cu−O2	2.133(5)	O2−Cu−N2a	96.9(3)
Cu−N1	2.001(7)	O2−Cu−N2b	94.4(6)
Cu−N2a	2.076(10)	O2−Cu−N3	95.0(2)
Cu−N2b	2.072(18)	N1−Cu−N2a	77.8(4)
Cu−N3	1.997(7)	N1−Cu−N2b	102.3(6)
C16−O1	1.266(9)	N1−Cu−N3	166.6(3)
C16[a]−O2	1.243(9)	N2a−Cu−N3	97.4(3)
Cu···Cu[a]	4.579(6)	N2b−Cu−N3	73.4(6)
O1−Cu−N1	90.7(3)	C16−O1−Cu	103.3(4)
O1−Cu−N2a	167.5(3)	Cu−O2−C16[a]	125.3(5)
O1−Cu−N2b	165.7(5)	O1−C16−O2[b]	121.9(7)
O1−Cu−N3	92.6(3)	O1−C16−C15	116.3(7)
O1−Cu−O2	89.6(2)	O2[b]−C16−C15	121.8(7)
$\{[Cu(L^2OO)(OClO_3)]\}_4\cdot MeCN$ (**3**)			
Cu−O1	1.958(5)	O1−Cu−O2[a]	86.8(2)
Cu−O2	1.973(5)	O1−Cu−O3	94.4(3)
Cu−O3	2.432(8)	O2−Cu−N1	88.2(2)
Cu−N1	2.028(7)	O2−Cu−N2	168.5(2)
Cu−N2	2.016(6)	O2[a]−Cu−O3	94.3(3)
C11−O1	1.259(8)	O3−Cu−N1	88.0(3)
C11−O2	1.256(8)	O3−Cu−N2	96.4(3)
Cu···Cu[a]	4.630(6)	N1−Cu−N2	96.5(3)
O1−Cu−N1	174.6(2)	C11−O1−Cu	124.9(5)
O1−Cu−N2	88.1(2)	C11−O2−Cu[b]	110.7(4)

[a] Symmetry operators for the generated atoms: $-x+3/2, y-1/2, -z+1/2$ for **1**; $-x, y-1/2, -z+3/2$ for **2**; and $-x+1, y+1/2, -z+1$ for **3**. [b] Symmetry operators for the generated atoms: $-x+3/2, y+1/2, -z+1/2$ for **1**; $-x, y+1/2, -z+3/2$ for **2** and $x-1/2, -y+1, -z+1$ for **3**.

(14) *DIAMOND* ver 2.1c; Crystal Impact GbR: Bonn, Germany, 1999.
(15) Steiner, T. *Angew. Chem., Int. Ed.* **2002**, *41*, 48–76.

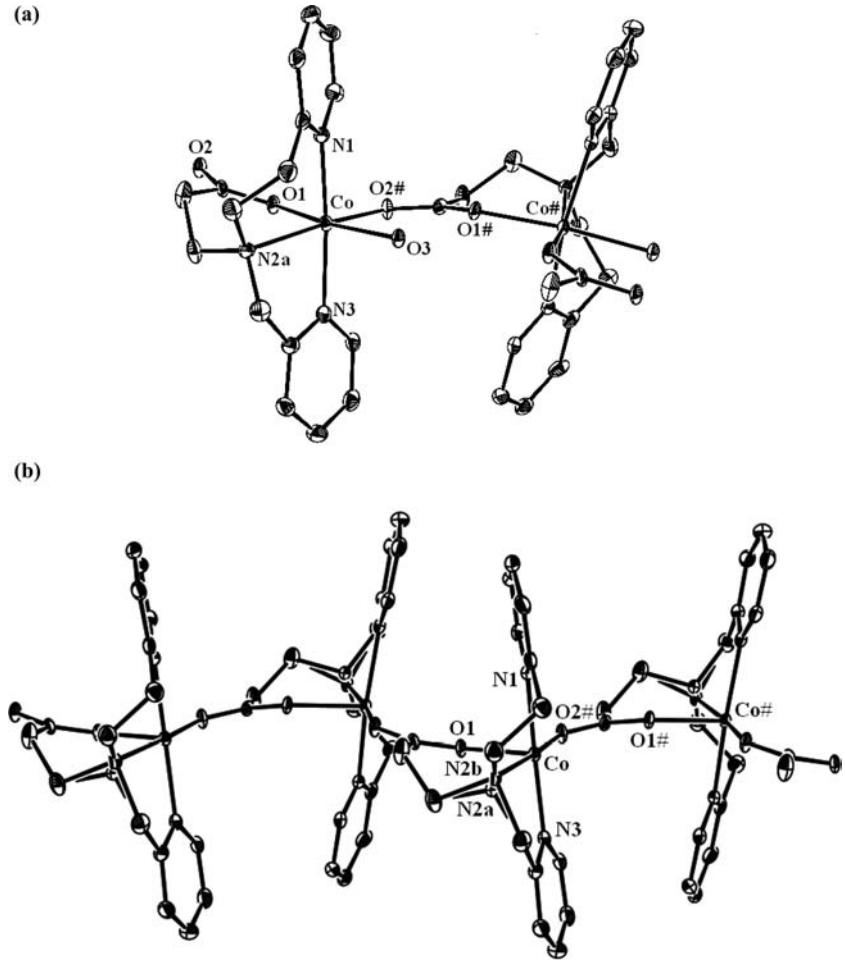

Figure 1. Perspective views of $[Co^{II}(L^1OO)(H_2O)][ClO_4]\cdot 2H_2O$ (**1**) [N(2) is distibuted over two positions; only donor atoms are labeled] (a) showing a metal coordination environment at two Co^{II} centers and (b) showing a 1D polymeric chain.

apparent. The cobalt atom in **1** is, however, displaced from the basal plane (defined by O1, O2#, N2a, and O3) by 0.0536(2) Å toward N(1). In **2**, each Cu^{II} ion assumes almost a perfect square-pyramidal $Cu^{II}N_3$(pyridylethyl-methylamine)O(monodentate and bridging carboxylate) coordination environment ($\tau = 0.010$).[16] The copper atom in **2** is displaced by 0.152 Å from the least-squares plane defined by the N_3O basal plane toward the carboxylate oxygen O(2). Moreover, the axial Cu−O(2) bond in **2** is not perfectly perpendicular to the CuN_3O plane but slightly bent off by 3.30°. Notably, in **1**, the Co−O(2#)−C(16)−O(1#)−Co# bridging network appreciably deviates from planarity [dihedral angle between the planes Co−O(2#)−C(16) and Co#−O(1#)−C(16): 13.66(5)°], and the angle between the plane of the carboxylate group coordinated to Co# and the CoN_3O plane is 74.41(5)°. In **2**, the dihedral angle between the planes Cu−O(1)−O(2#) and Cu#−O(2#)−O(1) is 2.60(1)°, and the plane of the carboxylate group coordinated to Cu# and the CuN_3O plane is 85.80(3)°.

The Co^{II}−O bond lengths [2.085(3)−2.153(3) Å] fall within the range typical of Co^{II}−O bond lengths (2.000−2.200 Å) in octahedral Co^{II} complexes.[6a] For the Co^{II}−N bonds, the trend is less prominent; the Co−N(amine) bonds [2.180(20)−2.226(10) Å] fall slightly short of the range reported (2.210−2.350 Å) and the Co−N(py) (py = pyridine) bonds [2.107(4)−2.116(3) Å] fall within the range of reported values (2.100−2.280 Å) for octahedral Co^{II} complexes.[6j,9l,o] The average $Cu-N_{py}$ bond distance of 1.998(7) Å is shorter by 0.1 Å than the average $Cu-N_{amine}$ distance of 2.098(14) Å. The Cu−N/O bond distances observed here are comparable with that reported for a closely similar structure.[6d,i]

$\{[Cu^{II}(L^2OO)(OClO_3)]\}_4\cdot$MeCN (3). The crystal structure of complex **3** consists of a tetranuclear $\{[Cu^{II}(L^2OO)(OClO_3)]\}_4$ core of $L^2OO(-)$ and copper(II) in a 1:1 ratio. A perspective view of **3** is presented in Figure 3. The ligand $L^2OO(-)$ acts as a tridentate ligand toward a Cu^{II} ion and acts as a monodentate bridging ligand toward a neighboring Cu^{II} center. Each Cu^{II} ion is coordinated by an ethylpyridyl nitrogen N(1), a tertiary amine nitrogen N(2), a carboxylate oxygen O(1) from the ligand $L^2OO(-)$, and an oxygen O(3) of ClO_4^-. The complex is formed from four $\{Cu^{II}(L^2OO)(OClO_3)\}$ units, bridged by four carboxylate oxygens from each unit. Each Cu^{II} ion is then bridged by a syn−anti carboxylate group [an oxygen atom O(2#) belongs to the carboxylate of an adjacent molecule]. All of the copper atoms in this structure have equivalent $Cu^{II}N_2$(pyridylethylamine)O(carboxylate)O′(perchlorate) coordination environ-

(16) Addison, A. W.; Rao, T. N.; Reedijk, J.; van Rijn, J.; Verschoor, G. C. *J. Chem. Soc., Dalton Trans.* **1984**, 1349–1356.

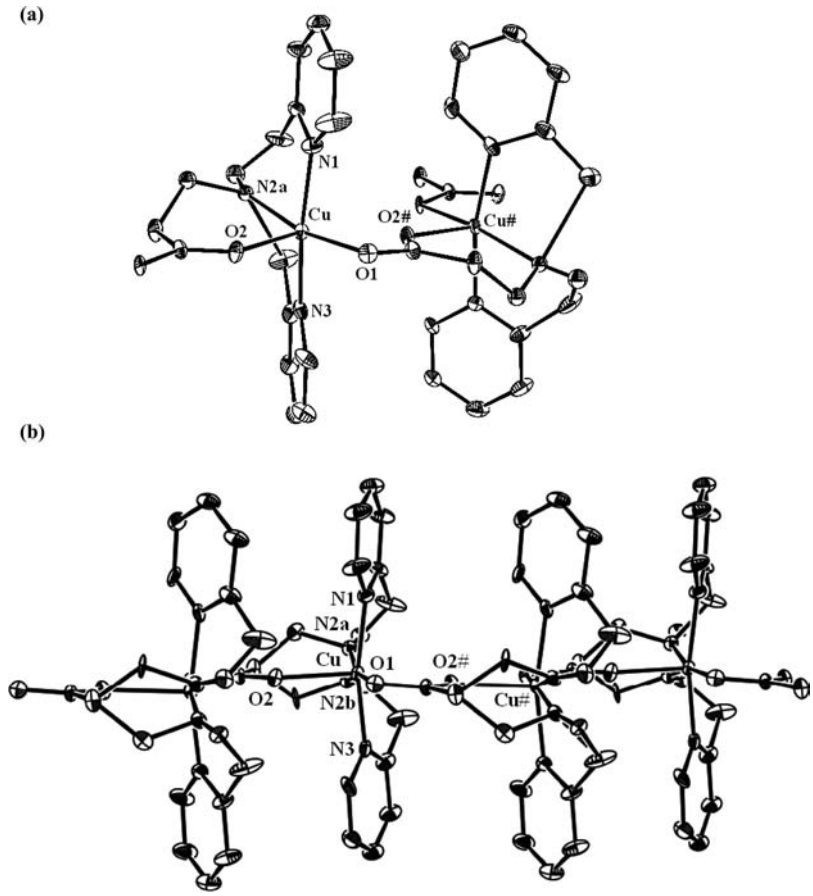

Figure 2. Perspective views of $[Cu^{II}(L^1OO)][ClO_4]\cdot 2H_2O$ (**2**) [N(2), C(7), and C(14) are distributed over two positions; only donor atoms are labeled] (a) showing a metal coordination environment at two centers and (b) showing a 1D polymeric chain.

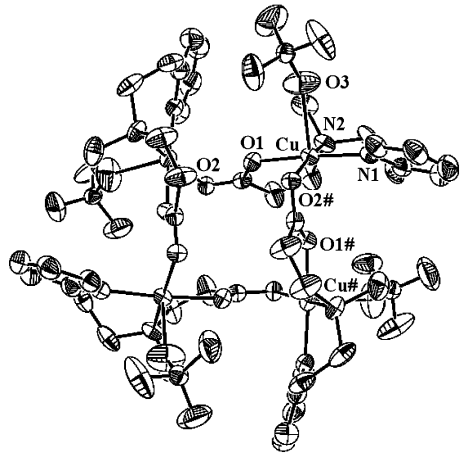

Figure 3. Perspective view of $\{[Cu^{II}(L^2OO)(OClO_3)]\}_4\cdot MeCN$ (**3**). Only donor atoms are labeled.

ments with similar geometric distortions. In essence, each copper center is five-coordinate, and the coordination geometry around each copper center is described as slightly distorted square pyramidal ($\tau = 0.100$).[16] For each copper(II) center, the base of the pyramid is defined by two nitrogen atoms [N(1) and N(2)], a carboxylate oxygen O(1) from the ligand $L^2OO(-)$, and a bridging carboxylate O(2#) from another ligand, and the apical position is occupied by the perchlorate oxygen O(3). The copper atom is displaced by 0.113 Å from the least-squares plane defined by the $CuN_2OO^{\#}$ basal plane toward the perchlorate oxygen O(3). The axial Cu−O(3) bond is not perfectly perpendicular to the CuN_3O plane but slightly bent off by 3.50°. Notably, at each copper center, the value of the dihedral angle between the plane of the carboxylate group and the basal plane is 89.32°. Each copper atom, in addition to the five bonding interactions discussed above, has a long Cu−O interaction at Cu···O(1#) = 2.742(7) Å. These distances are nonbonding, but the oxygen atoms are sterically placed to block the "sixth" coordination site in an "octahedral" arrangement of ligands around the metal ions.

The Cu−N/O bond lengths around each copper in **3** follow the usual pattern. Thus, the axial bond lengths for each copper [Cu−O(3) = 2.432(5) Å] are always longer than the corresponding four basal planes [Cu−N(1)/N(2)/O(1)/O(2): 2.027(5)/2.016(8)/1.957(4)/1.973(6) Å].

Interestingly, the carboxylate-bridging groups and $Cu^{II}(N_3O)$ units form a 16-membered ring $(-Cu-O-C-O)_4$ with the four copper ions located at the corners of a flattened tetrahedron. The Cu···Cu separations are ~6.510 Å along the two flattened edges and ~4.630 Å along the edges. In essence, the ligand L^2OO^- is coordinated to Cu^{II} and folded in such a way that the tetranuclear structure was assembled, as reported with other carboxylate-based ligands.[6b,c,7]

Noncovalent Interactions. A closer inspection of the crystal packing diagrams of **1** and **3** reveals that these compounds are engaged in secondary interactions. 1D coordination polymeric complex **1** is engaged in extensive

$\pi-\pi$ stacking interactions involving alternate pyridine rings of adjacent 1D chains, leading to the formation of 2D network structure (Figure S5, Supporting Information). Notably, the two pyridine rings are in a staggered conformation and the centroid−centroid distance of stacking pyridine rings is 3.6794(14) Å, with a perpendicular distance between the rings of 3.3125 Å´. The dihedral angle between the planes is 0.0°, and the displacement angle is $\beta = 24.432°$. These interaction parameters indicate strong parallel displaced $\pi-\pi$ stacking between the pyridine rings.[17] Complex **3** is engaged in C−H···O hydrogen-bonding interactions [C8−H8···O5, 2.413 Å and C8···O5, 3.4568(16) Å (symmetry: x, y, $-1 + z$); C8−H8···O5, 161.54(2)° (symmetry: x, y, $1 + z$)] involving the oxygen atom of the Cu^{II}-bound perchlorate anion and hydrogen atom of methyl group of an adjacent tetranuclear unit, leading to the formation of a 2D network structure (Figure S6, Supporting Information). The C−H···O hydrogen-bonding parameters observed in this work are in good agreement with literature tabulations[18] and literature precedents,[19] including our own findings.[20] These can be classified as intermediate contacts (2.439−2.598 Å), which are appreciably shorter than the sum of van der Waals radii for the H and the neutral O atoms (2.72 Å).[19]

Absorption Spectra. The absorption spectrum of **1** in H_2O clearly supports the presence of six-coordinate Co^{II} centers in solution (Figure S2, Supporting Information). Three spin-allowed d−d transitions are expected for octahedral Co^{II}, unless the field strength of the ligands is such that $^4A_{2g}$ and $^4T_{1g}(P)$ terms have the same energy.[21] The assignment of ν_1 (9524 cm^{-1}) as a $^4T_{1g}(F) \rightarrow {}^4T_{2g}(F)$ transition is unequivocal, and the ν_2 (20 408 cm^{-1}) is assigned as a $^4T_{1g}(F) \rightarrow {}^4T_{1g}(P)$ transition. From these values, one obtains the ligand-field parameters $Dq = 1072$ cm^{-1} (octahedral ligand-field strength) and $B = 806$ cm^{-1} (Racah parameter) for **1**. Still higher energy transitions are due to metal-perturbed intraligand transitions. The absorption spectrum of **2** in H_2O clearly supports the presence of five-coordinate Cu^{II} centers in solution (Figure S3, Supporting Information). The absorptions at 15 873 cm^{-1} and 10 362 cm^{-1} are characteristic of $d_{xy} \rightarrow d_{x^2-y^2}$ and $d_{z^2} \rightarrow d_{x^2-y^2}$ transitions, respectively, in a tetragonal ligand field ($Dq \approx 1580$ cm^{-1}), in which the Cu^{II} ions have a distorted square-pyramidal coordination environment (cf. X-ray structure). The absorption spectral feature of **3** in CH_3CN (Figure S4, Supporting Information), however, does not support the presence of five-coordinate Cu^{II} centers in solution. The asymmetric band at 15 748 cm^{-1} suggests the presence of a distorted octahedral stereochemistry around Cu^{II}. Two possibilities exist. Either the low-energy transition falls out of the range for which the spectrum was recorded or each Cu^{II} ion, in addition to five bonding interactions, has a long Cu−O interaction at Cu···O(1#) = 2.7429(7) Å (see above).

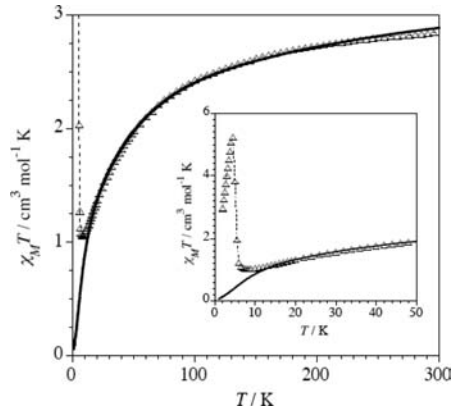

Figure 4. Plot of $\chi_M T$ vs T for a powdered sample of $[Co^{II}(L^1OO)(H_2O)][ClO_4]\cdot 2H_2O$ (**1**). The solid line represents the best simulation obtained with the model described in the text. Inset: Zoom of the dependence of the $\chi_M T$ product of **1** in the low temperature (<10 T) region under 0.01 T.

Magnetic Properties. The temperature dependence of the $\chi_M T$ product for **1** [χ_M being the magnetic susceptibility per Co^{II} ion] is shown in Figure 4. At room temperature, the value of $\chi_M T$ is 2.50 cm^3 mol^{-1} K, which is greater than that expected for a high-spin Co^{II} ion through the spin-only formula (1.87 cm^3 mol^{-1} K with $g = 2.0$). This is due to the occurrence of an unquenched orbital contribution typical of the $^4T_{1g}$ ground-state in octahedral high-spin Co^{II} complexes.[22] Upon cooling, the $\chi_M T$ value continuously decreases, reaching a minimum with a value of 1.0 cm^3 mol^{-1} K at 10 K. This value is lower than that expected for a magnetically isolated Co^{II} ion ($\chi_M T \approx 1.73$ cm^3 mol^{-1} K for an effective spin doublet with $g_0 \approx 4.3$),[23] indicating the occurrence of an antiferromagnetic exchange interaction. Below 9 K, there is an abrupt increase to a maximum at 4.5 K ($\chi_M T = 5.2$ cm^3 mol^{-1} K under an applied field of 100 G); then, $\chi_M T$ decreases linearly with T (see inset of Figure 4). The decrease of $\chi_M T$ in the 10−300 K temperature range is due to an *intrachain* antiferromagnetic exchange interaction between the Co^{II} ions as well as to the depopulation of the higher-energy spin−orbit levels of the six-coordinated Co^{II} centers. The abrupt increase of $\chi_M T$ below 9 K is due to a ferromagnetic phase transition related to a spin canting[6m,8,9a−d,f,l,m,o] with a critical temperature $T_c = 5$ K. Its occurrence is supported by the field-cooled magnetization (Figure 5), hysteresis loop (Figure 6), and ac susceptibility measurements (Figure S7, Supporting Information). Upon cooling in a low field ($H = 100$ G), the magnetization of **1** exhibits a sharp transition below 9 K ($T_c = 5$ K; see Figure

(17) (a) Janiak, C. *J. Chem. Soc., Dalton Trans.* **2000**, 3885–3896. (b) Reger, D. L.; Gardinier, J. R.; Semeniuc, R. F.; Smith, M. D. *Dalton Trans.* **2003**, 1712–1718. (c) Reger, D. L.; Semeniuc, R. F.; Smith, M. D. *Cryst. Growth Des.* **2005**, *5*, 1181–1190. (d) Agrifoglio, G.; Karam, A. R.; Catarí, E. L.; González, T.; Atencio, R. *Acta Crystallogr., Sect. E.* **2005**, *61*, 2613–2616.
(18) Taylor, R.; Kennard, O. *J. Am. Chem. Soc.* **1982**, *104*, 5063–5070.
(19) Brammer, L.; Desiraju, G. R. *Perspectives in Supramolecular Chemistry − Crystal Design: Structure and Function*; Wiley: Chichester, U.K., 2003; Vol. *7*; pp 1−75.
(20) Balamurugan, V.; Hundal, M. S.; Mukherjee, R. *Chem.—Eur. J.* **2004**, *10*, 1683–1690.
(21) (a) Cotton, F. A.; Wilkinson, G.; Bochmann, M. *Advanced Inorganic Chemistry*, 6th ed.; Wiley: New York, 1999. (b) Dou, Y.-S. *J. Chem. Educ.* **1990**, *67*, 134–135. (c) Hathaway, B. J. *Structure Bonding (Berlin)* **1991**, *57*, 55–118.
(22) (a) Figgis, B. N.; Gerloch, M.; Lewis, J.; Mabbs, F. E.; Webb, G. A. *J. Chem. Soc. A* **1968**, 2086–2093. (b) Gerloch, M.; Quested, P. N. *J. Chem. Soc. A* **1971**, 3729–3756. (c) Mabbs, F. E.; Machin, D. J. *Magnetism in Transition Metal Complexes*; Chapman and Hall: London, 1973.
(23) Lines, M. E. *J. Chem. Phys.* **1971**, *55*, 2977–2984.

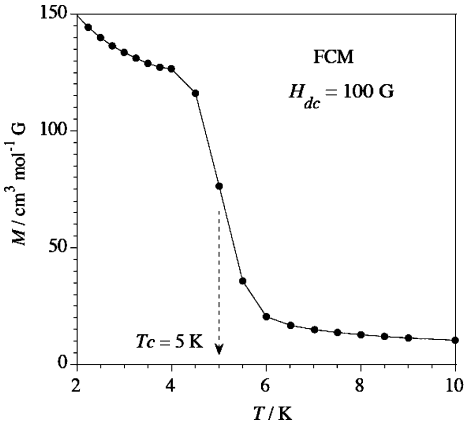

Figure 5. Field-cooled magnetization plot for $[Co^{II}(L^1OO)(H_2O)][ClO_4]\cdot 2H_2O$ (**1**).

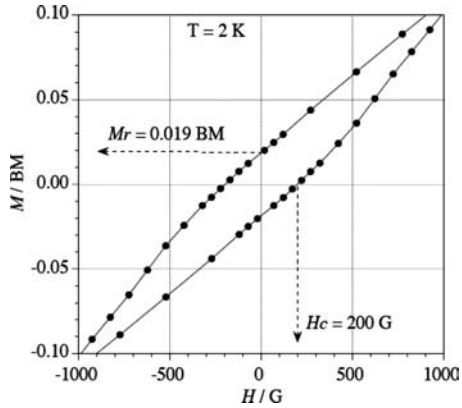

Figure 6. Hysteresis loop of the magnetization for $[Co^{II}(L^1OO)(H_2O)][ClO_4]\cdot 2H_2O$ (**1**).

5), and then it approaches a saturation value of 140 cm^3 mol^{-1} G (0.025 μ_B). This value is far away from that expected for a high-spin Co^{II} ion, indicating the presence of a small canting angle.[8,9] From this saturation value, a canting angle [$= 2\ sin^{-1}(M_c/2M_s)$, where M_c is the saturation value at 100 G and M_s ($= gS$) is the expected saturation magnetization if all the moments are aligned ferromagnetically][6m,8] of about 0.5° (considering $g = 2$ and $S = 3/2$) can be estimated. The T_c is taken here as the maximum of the slope dM/dT, which coincides with the maxima observed for in-phase (χ_M') and out-of-phase (χ_M'') ac magnetic susceptibilities (see Figure S7, Supporting Information). The magnetic hysteresis loop is shown in Figure 6. At $T = 2$ K, the values of the coercive field (H_c) and remnant magnetization (M_r) are 200 G and 0.019 μ_B, respectively.

In order to determine the *intrachain* exchange interaction in **1** in the temperature range 10−300 K, we have used an approach that we reported recently.[24] This approach is based on a perturbation model where the magnetic coupling only operates between the ground Kramers doublets, which are considered as effective spins $S_{eff} = 1/2$. The exchange interactions in the excited doublets are neglected, and thus, their magnetic properties are considered as those of the magnetically isolated ions. The contribution of these excited doublets to the magnetic properties of ground one is taken into account by a second-order perturbation theory. This introduces a dependence on J, λ, α, and Δ in the Landé factor of the ground doublet, g_0, where J is the isotropic exchange interaction, λ is the spin−orbit coupling, α is the orbital reduction factor defined as $\alpha = kA$ [where k considers the reduction of the spin−orbit coupling due to covalency and A is a measure of the crystal-field strength, and it takes into account the admixture of the upper $^4T_{1g}(^4P)$ state into the $^4T_{1g}(^4F)$ ground state],[22] and Δ is the energy gap between the singlet $^4A_2$ and doublet ^4E levels due to the splitting of the orbital triplet $^4T_{1g}$ ground state under an axial distortion. All of these effects are incorporated into a function named $G(T,J)$ which replaces the value of the g_0 Landé factor of the ground Kramers doublet. This approach is valid in the limit of the weak magnetic coupling as compared to the spin−orbit coupling, $|J/\lambda| < 0.1$, and it is able to analyze the magnetic data of high-spin Co^{II} compounds in the whole temperature range. Following this approach, we can treat the Co^{II} ions as effective spin doublets ($S_{eff} = 1/2$) which are related to the real spins ($S = 3/2$) by $S_{eff} = (3/5)S$. For that, we replace the value of the g_0 Landé factor of the ground Kramers doublet with the $G(T,J)$ function, which is calculated as described.[24]

In this sense and from a magnetic point of view, complex **1** can be viewed as a uniform chain of antiferromagnetically interacting spin doublets. The numerical expression derived by Bonner and Fisher[25] (eq 1) can then be used to analyze the magnetic susceptibility of **1**, where $x = (25/9)|J|/kT$ and the g factor is replaced by the $G(T,J)$ function.

$$\chi_M = \frac{N\beta^2 g^2}{kT}\frac{0.25 + 0.074975x + 0.075235x^2}{1.0 + 0.9931x + 0.172135x^2 + 0.757825x^3} \quad (1)$$

The corresponding analysis of magnetic data (for $T > 10$ K) of **1** through eq 1 leads to the following set of best-fit parameters: $J = -2.65(2)$ cm^{-1}, $\lambda = -163(5)$ cm^{-1}, $\Delta = 525(10)$ cm^{-1}, and $\alpha = 1.13(1)$. For the free ion, the value of λ is -170 cm^{-1}.[6m] The theoretical curve (solid line in Figure 4) reproduces quite well the magnetic data in the temperature range 10−300 K. The low value of the $|J/\lambda|$ quotient (0.016) justifies the use of the above approach. From the ligand-field parameters of **1** ($Dq = 1072$ cm^{-1} and $B = 806$ cm^{-1}; see above), a value of $A = 1.39$ can be estimated,[24,26,27] and so, $k = 0.81$. It is worth mentioning here that A assumes a value of 1.5 for a weak crystal field and 1.0 for a strong crystal field.[6m,24] The values of the λ, A, k, and Δ parameters lie within the range of those observed in other six-coordinated high-spin Co^{II} complexes.[26,28]

(24) Lloret, F.; Julve, M.; Cano, J.; Ruiz-García, R.; Pardo, E. *Inorg. Chim. Acta* **2008**, *361*, 3432–3445.

(25) Bonner, J. C.; Fisher, M. E. *Phys. Rev. A: At., Mol., Opt. Phys.* **1964**, *135*, 640–658.

(26) Herrera, J. M.; Bleuzen, A.; Dromzée, Y.; Julve, M.; Lloret, F.; Verdaguer, M. *Inorg. Chem.* **2003**, *42*, 7052–7059.

(27) Mishra, V.; Lloret, F.; Mukherjee, R. *Inorg. Chim. Acta* **2006**, *359*, 4053–4062.

(28) (a) De Munno, G.; Julve, M.; Lloret, F.; Faus, J.; Caneschi, A. *J. Chem. Soc., Dalton Trans.* **1994**, 1175–1183. (b) De Munno, G.; Poerio, T.; Julve, M.; Lloret, F.; Viau, G. *New J. Chem.* **1998**, 299–305. (c) Cañadillas-Delgado, L.; Fabelo, O.; Pasán, J.; Delgado, F. S.; Lloret, F.; Julve, M.; Ruiz-Pérez, C. *Inorg. Chem.* **2007**, *46*, 7458–7465.

Scheme 1

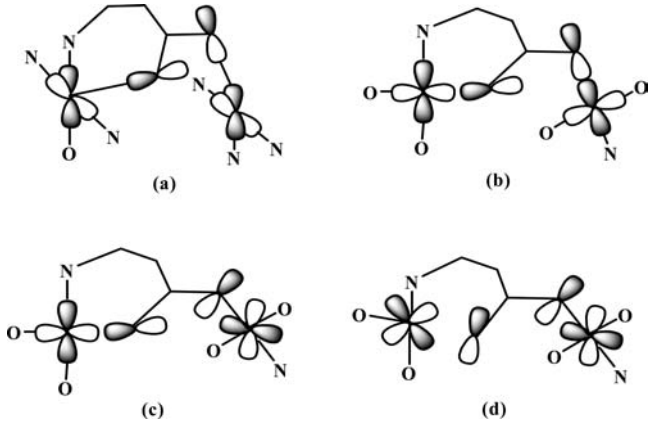

The $\chi_M T$ versus T plot for **2** is shown in Figure S8, Supporting Information. Upon cooling, the $\chi_M T$ value remains constant up to 40 K ($\chi_M T = 0.40$ cm^3 mol^{-1} K); then, it continuously decreases to reach 0.30 cm^3 mol^{-1} K at 2.0 K. This behavior indicates the occurrence of a weak *intrachain* exchange interaction. The experimental data were fitted using eq 1 with $x = |J|/kT$ and g being the Landé factor of the Cu^{II} ion. The best-fit parameters are $g = 2.07(1)$ and $J = -0.66(1)$ cm^{-1}. The weaker antiferromagnetic exchange interaction in **2** with respect to that observed for **1** (10−300 K range) must be attributed to the fact that the carboxylate bridge in **2** connects an equatorial position (short bond) of a Cu^{II} ion with the apical one (long bond) of the next-neighbor Cu^{II} ion (see Scheme 1a); whereas, in **1**, the carboxylate bridge connects two short bonds (Scheme 1b).

The global feature of the magnetic behavior of **3** (Figure 7) is characteristic of a weak ferromagnetic exchange interaction, arising from intramolecular interactions between the four Cu^{II} ions. The $\chi_M T$ value of 1.60 cm^3 mol^{-1} K at 300 K is as expected for four magnetically quasi-isolated spin doublets. This value continuously increases and reaches a maximum of 2.96 cm^3 mol^{-1} K (4.87 μ_B) at 4.0 K, and after that it decreases at lower temperatures (2.88 cm^3 mol^{-1} K at 2.0 K). In principle, this decrease can be attributed to either intermolecular antiferromagnetic interactions (θ), to zero-field splitting (D) effects within the ground quintet spin state ($S = 2$), or to both factors.[29a]

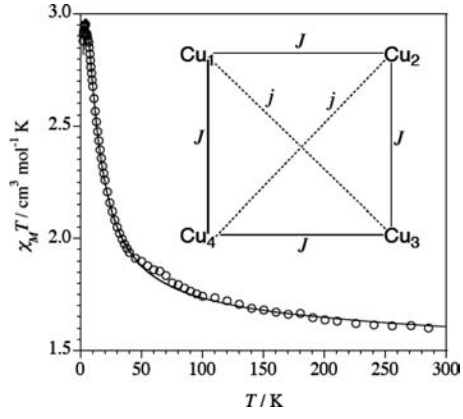

Figure 7. Plot of $\chi_M T$ versus T for a powdered sample of $\{[Cu^{II}(L^2OO)(OClO_3)]\}_4 \cdot MeCN$ (**3**). The solid line represents the best theoretical fit, described in the text.

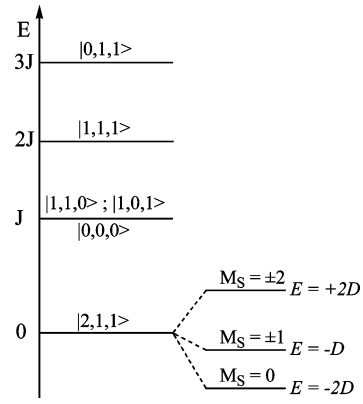

Figure 8. Energy levels for **3**, based on a perturbation approach for the zero-field splitting on the $S = 2$ ground state. The states are represented by the $|S, S_{13}, S_{24}>$ functions, where $S = S_{13} + S_{24}$, $S_{13} = S_1 + S_3$, and $S_{24} = S_2 + S_4$, and their energies are calculated by using the Hamiltonian, $H = -J(S_1S_2 + S_3S_3 + S_3S_4 + S_1S_4)$ (see inset in Figure 7 with $j = 0$).

Assuming that the decrease of $\chi_M T$ below 4.0 K is mainly due to the zero-field splitting of the quintet ground state and that this state is well separated in energy from the next excited spin states (that is $D \ll J$), such as indicated in Figure 8, eq 2 can be deduced for the magnetic susceptibility to describe the magnetic behavior of **3**:[30]

$$\chi_{\parallel} = \frac{2N\beta^2 g_{\parallel}^2}{kT}\left\{\frac{F_D^{\parallel} + F_J}{Z}\right\} \tag{2a}$$

$$\chi_{\perp} = \frac{2N\beta^2 g_{\perp}^2}{kT}\left\{\frac{F_D^{\perp} + F_J}{Z}\right\} \tag{2b}$$

$$\chi_M = \frac{\chi_{\parallel} + 2\chi_{\perp}}{3} \tag{2c}$$

where

$$Z = \exp(2D/kT) + 2\exp(D/kT) + 2\exp(-2D/kT) + 7\exp(-J/kT) + 3\exp(-2J/kT) + \exp(-3J/kT)$$

$$F_J = 2\exp(-J/kT) + \exp(-2J/kT)$$

$$F_D^{\parallel} = \exp(D/kT) + 4\exp(-2D/kT)$$

Due to the presence of a tetracopper(II) square (Figure 3), only one exchange coupling parameter J (inset of Figure 7) has been considered to fit the data through eq 2.[29] The best-fit parameters are $g = 2.08(1)$, $|D| = 0.8(1)$ cm^{-1}, and $J = +12.2(2)$ cm^{-1}. The low value of the ratio D/J (= 0.06) allows us to use eq 2. As indicated above, the decrease of $\chi_M T$ at low temperatures could also be attributed to intermolecular interactions. In this sense, we can reproduce the $\chi_M T$ curve by using a Weiss constant (θ), in the form of (T

(29) (a) Rodriguez-Martín, Y.; Ruiz-Pérez, C.; Sánchiz, J.; Lloret, F.; Julve, M. *Inorg. Chim. Acta* **2001**, *318*, 159–165. (b) Rodriguez-Martín, Y.; Hernández-Molina, M.; Delgado, F. S.; Pasán, J.; Ruiz-Pérez, C.; Sánchiz, J.; Lloret, F.; Julve, M. *CrystEngComm* **2002**, *4*, 440–446. (c) Rodríguez-Martín, Y.; Hernández-Molina, M.; Delgado, F. S.; Pasán, J.; Ruiz-Pérez, C.; Sánchiz, J.; Lloret, F.; Julve, M. *CrystEngComm* **2002**, *4*, 522–535.

(30) Ruiz, R.; Lloret, F.; Julve, M.; Faus, J.; Muñoz, M. C.; Solans, X. *Inorg. Chim. Acta* **1993**, *213*, 261–268.

(31) (a) Sánchiz, J.; Rodríguez-Martín, Y.; Ruiz-Pérez, C.; Mederos, A.; Lloret, F.; Julve, M. *New J. Chem.* **2002**, *26*, 1624–1628. (b) Delgado, F. S.; Sánchiz, J.; Ruiz-Pérez, C.; Lloret, F.; Julve, M. *Inorg. Chem.* **2003**, *42*, 5938–5948.

Scheme 2

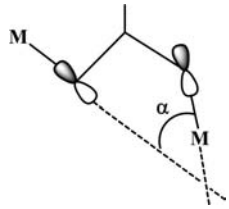

$-\theta$). The fit through eq 2 with $D = 0$ leads to the same values of J and g, θ being -0.3 K. So, due to the possibility of occurrence of some intermolecular interaction in **3** (see above), the D value given above must be considered as the higher limit for this parameter. The value of J is comparable to reported systems of similar tetracopper(II) complexes.[29,31]

Rationalization of Observed Magnetic Behavior. Systematic alternation of the relative orientation of the neighboring metal coordination sphere (two slanted basal planes of Co^{II} ions with single-ion anisotropy; cf. X-ray structure) must be the cause for the spin-canted antiferromagnetic exchange interaction observed in **1**. Notably, in **1**, the Co−O−C−O−Co# bridging network appreciably deviates from planarity [dihedral angle: 13.66(5)°], and the angle between the plane of the carboxylate group coordinated to Co# and the CoN_3O plane is 74.41(5)°. As indicated above, the weak antiferromagnetic exchange coupling observed in **2** can be easily understood given the fact that the carboxylate bridge in **2** connects one equatorial position of a Cu^{II} ion with the axial position of the adjacent copper (Scheme 1a). The exchange interaction in the other cases (**1** and **3**) is strong because a carboxylate bridge links two adjacent equatorial positions (Scheme 1b). In order to understand the different nature of the exchange interaction in **1** (antiferromagnetic) and **3** (ferromagnetic), it is important to take into account the fact that the syn−anti carboxylate bridge mediates weak exchange interactions, either ferro- or antiferromagnetic.[6d,f,l,7a,b,d,f] From this perspective, Scheme 2 is illustrative: when the α value is close to 90°, a ferromagnetic exchange interaction is expected, while smaller values for this angle lead to an antiferromagnetic exchange coupling. In fact, the prediction is in conformity with the observed values of α (∼51.76° for **1** and ∼71.77° for **3**). The out-of-plane deviations in the M−O−C−O#−M# skeleton (see above) also play a relevant role. In the case of **3**, there is only one magnetic orbital on each metal center ($d_{x^2-y^2}$ type), as shown in Scheme 1b, whereas for **1**, three magnetic orbitals ($d_{x^2-y^2}$, d_{z^2}, and d_{xy}) are present on each metal center. Consequently, nine combinations between magnetic orbitals occur in **1**. Six of them (those involving different types of magnetic orbitals, for instance, Scheme 1c describing the coupling between $d_{x^2-y^2}$ and d_{xy} magnetic orbitals) always lead to a net overlap and to an antiferromagnetic exchange interaction,[32] whereas the remaining three (two of them being shown in Scheme 1b and d) can mediate ferro- or antiferromagnetic exchange interaction depending on the α value (Scheme 2) discussed above. The structural parameters of **1** and **3** are similar, and hence the antiferromagnetic exchange coupling observed in **1** can be mainly attributed to the occurrence of these six antiferromagnetic contributions (Scheme 1c).

Summary and Concluding Remarks

Three new complexes [two 1D coordination polymers and a discrete tetracopper(II) cluster] supported by carboxylate-appended (2-pyridyl)alkylamine ligands have been structurally and magnetically characterized. Structural analyses provide examples of the ligand denticity-controlled self-assembly process leading to 2D architecture construction ($\pi\cdots\pi$ and C−H···O interactions), utilizing the coordination modes of the chosen ligands.[6d,i] Temperature-dependent magnetic susceptibility measurements reveal (i) spin-canted antiferromagnetism in the 1D coordination polymer of Co^{II}, (ii) weak antiferromagnetic exchange interaction in the 1D coordination polymer of Cu^{II}, and (iii) ferromagnetic exchange interaction in the tetracopper(II) complex. The successful syntheses of these complexes enriched the syn−anti carboxylate-bridged complexes not only structurally but magnetically as well. Future efforts will investigate how the stereochemical demand of this class of ligands would direct the molecular shape and control the magnetic properties of the resulting complexes. Such an endeavor is on in this laboratory.

Acknowledgment. This work is supported by the Department of Science & Technology, Government of India, and by the Ministerio de Educación y Ciencia (MEC, Spain; projects CTQ2007-61690 and Consolider-Ingenio in Molecular Science CSD2007-00010). H.A. gratefully acknowledges the award of SRF by Council of Scientific & Industrial Research, Government of India. Comments of the reviewers were very helpful at the revision stage.

Supporting Information Available: CIF files for **1**, **2**, and **3**; donor atom disorder in **2** (Figure S1); UV−vis spectra of **1**−**3** (Figures S2−S4); noncovalent interaction among each polymeric chain in **1** (Figure S5); noncovalent interaction among tetranuclear core in **3** (Figure S6); temperature dependence of the real (χ') and imaginary parts (χ'') of ac susceptibility for **1** (Figure S7); magnetism of **2** (Figure S8). This material is available free of charge via the Internet at http://pubs.acs.org.

IC800861M

(32) Cuevas, A.; Kremer, C.; Suescum, L.; Russi, S.; Mombru, A. W.; Lloret, F.; Julve, M.; Faus, J. *Dalton Trans.* **2007**, 5305–5315.